Ceramics International 47 (2021) 28675–28684

Contents lists available at ScienceDirect

Ceramics International

journal homepage: www.elsevier.com/locate/ceramint

A low-sintering temperature microwave dielectric ceramic for 5G LTCC applications with ultralow loss

Dong Wang [a,b], Lingxia Li [a,b,*], Mingkun Du [a,b,**], Yu Zhan [a,b]

[a] School of Microelectronics, Tianjin University, Tianjin, 300072, China
[b] Tianjin Key Laboratory of Imaging and Sensing Microelectronic Technology, Tianjin University, Tianjin, 300072, China

ARTICLE INFO

Keywords:
Li_2TiO_3
Microwave dielectric properties
LTCC applications

ABSTRACT

In next-generation mobile and wireless communication systems, low sintering temperature and excellent dielectric properties are synergistic objectives in the application of dielectric resonators/filters. In this work, $Li_2Ti_{0.98}Mg_{0.02}O_{2.96}F_{0.04}$–1 wt% Nb_2O_5 (LTMN) ceramics were fabricated, and their sintering temperature was successfully lowered from 1120 °C to 750 °C by adjusting the mass ratio of B_2O_3–CuO (BC) additive. The optimum dielectric properties ($\varepsilon_r \sim 24.44$, $Q \times f \sim 60{,}574$ GHz and $\tau_f \sim 22.8$ ppm/°C) were obtained in BC-modified LTMN ceramics sintered at 790 °C. Even if their sintering temperature was lowered to 750 °C, the lowest temperature among the Li_2TiO_3-based dielectric ceramics currently used for LTCC technology, excellent dielectric properties ($\varepsilon_r \sim 23.77$, $Q \times f \sim 51{,}636$ GHz) were still maintained. Additionally, no extra impurity phase was detected in BC-modified LTMN ceramics co-fired with Ag at 790 °C, indicating that BC-modified LTMN ceramics have a bright prospect in high-performance LTCC devices for 5G applications.

1. Introduction

With the rapid development of fifth-generation (5G) communication technology, the application of Massive MIMO (large-scale antenna arrays) and AAU (active antenna unit) RF technology has put higher requirements on the miniaturization and integration of 5G base stations [1].

Low temperature co-fired ceramic (LTCC) technology has been proven to be one of the most effective ways to reduce device size and circuit area. Many high-performance communication devices have been manufactured, such as LC filters, GPS antennas, phase-controlled radars, circuit substrates, and dielectric resonators etc. [2–4]. It is well known that the electromagnetic wave oscillation occurs inside the dielectric ceramic devices, and the quality factor of devices is closely related to dielectric loss, so, higher requirements for LTCC materials are proposed [1]: (1) appropriate dielectric constant (ε_r:5–25); Suitable dielectric constant is beneficial to reducing device size and realize lower time-delay as the following equations described [5,6].

$$\lambda_r = \frac{\lambda_0}{\sqrt{\varepsilon_r}} \tag{1}$$

where λ_0 and λ_r are wavelength in vacuum and dielectric with ε_r value, respectively.

$$T_{PD} = \frac{l\sqrt{\lambda_r}}{C} \tag{2}$$

where l is transmission distance, C is the speed of light in vacuum, and T_{PD} is the time-delay of signal propagation. (2) low dielectric loss ($Q = 1/\tan\delta$, $Q \times f > 50{,}000$ GHz); Improved $Q \times f$ value is beneficial to reducing crosstalk between signal channels, and increasing the power capacity of devices, which is significantly required performance by 5G communication devices [5]. (3) near-zero temperature coefficient of resonant frequency (τ_f); A near-zero temperature coefficient of resonant frequency means that the operating frequency of devices will be limitedly affected by temperature, indicating a higher temperature-reliability [7–9]. What's more, an important requirement for LTCC is the ability to co-fire with Ag electrodes below 961 °C without additional chemical reactions [3,10,11]. However, traditional microwave dielectric ceramics are hard to meet the requirement of LTCC technology due to a higher sintering temperature.

Currently, low sintering temperature (<961 °C) materials for LTCC devices can be prepared by four methods. Firstly, glass-ceramics/glass-

* Corresponding author. School of Microelectronics, Tianjin University, Tianjin, 300072, China.
** Corresponding author. School of Microelectronics, Tianjin University, Tianjin, 300072, China.
E-mail addresses: Li_ling_xia_tju@163.com (L. Li), dmkun@tju.edu.cn (M. Du).

https://doi.org/10.1016/j.ceramint.2021.07.027
Received 25 May 2021; Received in revised form 25 June 2021; Accepted 2 July 2021
Available online 3 July 2021

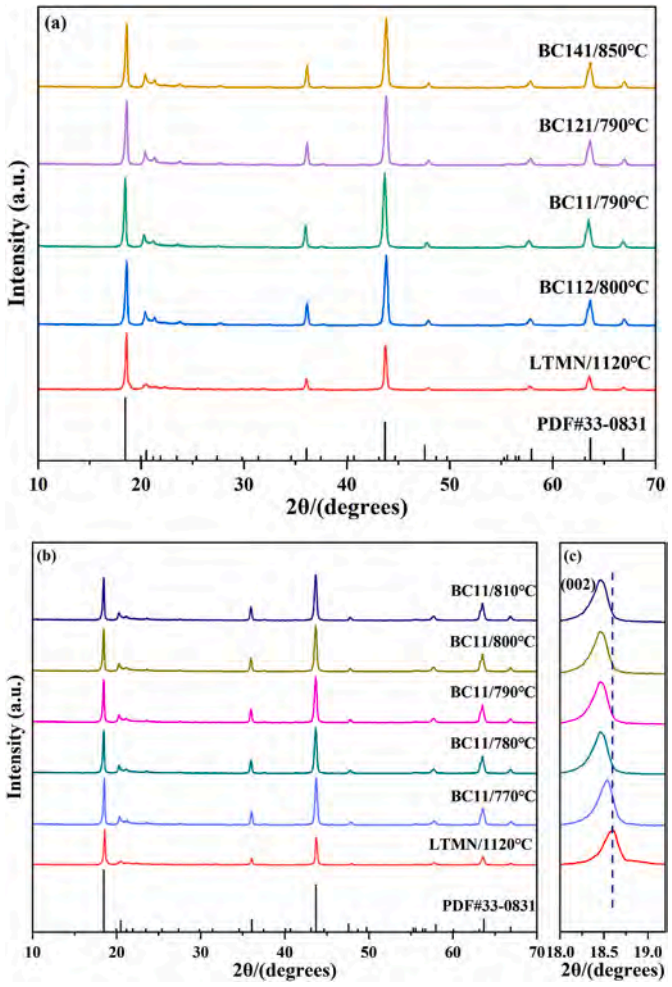

Fig. 1. (a) XRD patterns of pure LTMN, BC112, BC11, BC121, and BC141 specimens sintered at optimum temperature for 4 h, respectively. (b) Variation of XRD pattern with sintering temperature for BC11 composition. (c) The locally enlarged diffraction peaks of (002) for all samples.

Table 1
Structure parameters of nine samples.

Samples	*a*(Å)	*b*(Å)	*c*(Å)	V_{cell} (Å^3)	R_p (%)	R_{wp} (%)
LTMN (1120 °C)	5.05670	8.77950	9.72754	425.38	8.19	10.68
BC112 (800 °C)	5.06053	8.76793	9.74077	425.96	8.35	11.24
BC121 (790 °C)	5.06375	8.76739	9.73953	426.12	7.79	10.17
BC141 (850 °C)	5.06261	8.77327	9.74138	426.21	8.84	10.59
BC11 (770 °C)	5.05623	8.77514	9.73712	425.71	8.75	9.91
BC11 (780 °C)	5.05184	8.78558	9.72908	425.95	8.47	10.26
BC11 (790 °C)	5.06252	8.77148	9.74220	426.09	7.16	9.48
BC11 (800 °C)	5.05454	8.77494	9.74593	426.11	8.45	9.63
BC11 (810 °C)	5.05796	8.78640	8.729453	426.16	8.99	10.05

ceramic composites are always used as the matrix phase and the sinterability and dielectric properties of matrix can be modified by other additives [3,12–16]. However, there still exists some shortcomings in the preparation process, such as composition volatizing and unstable dielectric performance. In addition, glass-ceramic composites are readily reacted with metal electrode, resulting in an inevitable decline of dielectric properties [17–20]. Secondly, novel microwave dielectric material systems are developed, which possess inherently low sintering temperature (such as MoO_3, TeO_2, P_2O_5, WO_3, Bi_2O_3 and V_2O_5-based compounds) [3,21–27]. However, there are many shortages in this method, such as costly (TeO_2), poisonous raw materials (V_2O_5, WO_3), low $Q \times f$ values (<50,000 GHz), and large τ_f values ($|\tau_f| > 30$ ppm/°C), which inhibit their wide application in LTCC devices. Thirdly, chemically synthesized nano-powders are used as raw materials to reduce the sintering temperature for ceramic densification. While it is a costly and time-consuming method. Fourthly, sintering aids/low melting-point oxides are added to ceramics, which is viewed as a widely used method to obtain high-performance materials of LTCC devices.

With the deepening of research on lithium-based dielectric ceramics, Li_2TiO_3 dielectric ceramic has attracted great attention due to its excellent dielectric properties ($\varepsilon_r = 21$–25, $Q \times f = 31{,}236$–71,000 GHz, and τ_f = 20–38.5 ppm/°C), relatively lower sintering temperature (~1230 °C), small density (~3.1 g/cm^3), and lower cost [1]. In our research group, $Li_2Ti_{0.98}Mg_{0.02}O_{2.96}F_{0.04}$–1 wt% Nb_2O_5 (abbreviated LTMN) ceramic sintered at 1120 °C with superior dielectric properties ($\varepsilon_r \sim 22.78$, $Q \times f \sim 116{,}927$ GHz, $\tau_f \sim 31.6$ ppm/°C) is developed, which is a promising candidate for LTCC applications. However, the sintering temperature of LTMN ceramic (1120 °C) is too high to co-fire with silver electrode (961 °C), so lowering its sintering temperature becomes the new research focus. Recently, some studies have shown that the sintering temperature of dielectric ceramics can be effectively reduced by adding a small amount of CuO/B_2O_3. For example, Ding et al. [28]revealed that adding B_2O_3–CuO (BC) to $3Li_2O$-Nb_2O_5-$6TiO_2$ could lower sintering temperature from 1125 °C to 900 °C with dielectric properties of $\varepsilon_r \sim 52$, $Q \times f \sim 12{,}000$ GHz, and $\tau_f \sim 32.3$ ppm/°C. Zhang et al. [29]found that the sintering temperature of $CoTiNb_2O_8$ added with CuO could be reduced from 1250 °C to 950 °C. Zhang et al. [30] reported that adding B_2O_3 to $Li_3Mg_2NbO_6$ could lower its sintering temperature from 1250 °C to 900 °C. Thus, reducing the sintering temperature of LTMN ceramic by the addition of B_2O_3 and CuO aids is hopeful and meaningful.

In this work, B_2O_3 and CuO mixture in different ratios was introduced to LTMN ceramic to achieve a lower sintering temperature. Microwave dielectric properties, microstructure, sintering characteristics and structural evolution were studied comprehensively. Moreover, chemical compatibility study was performed by 25 wt% Ag and BC-doped LTMN ceramics cofired at the optimum sintering temperature.

2. Experimental procedure

Some raw materials for synthesizing LTMN ceramic of Li_2CO_3, MgF_2 (98.0%, 99.99%, Yuan Li), TiO_2 (99.0%, Peng Da) were pre-prepared according to the stoichiometric formulation $Li_2Ti_{0.98}Mg_{0.02}O_{2.96}F_{0.04}$ (abbreviated LTM). Firstly, these oxide powders were weighed with an electronic balance according to the molecular formula, then ball-milled with ethanol in a nylon tank for 12 h. Secondly, the slurries were dried in a thermostat, and calcined at 800 °C for 4 h. Thirdly, the calcined powders were mixed with 1 wt% Nb_2O_5 (99.99%, Jiu Jiang) and 1 wt% B_2O_3–CuO (98.0%–99.0%, Jiang Tian, Yuan Li; abbreviated BC), and re-milled in ethanol medium for 12 h. The mass ratio of CuO to B_2O_3 (*x*:*y*) was 1.0:1.2, 1.0:1.0, 1.2:1.0 and 1.4:1.0, and BC-doped LTMN samples were named BC112 (*x*:*y* = 1.0:1.2), BC11 (*x*:*y* = 1.0:1.0), BC121 (*x*:*y* =

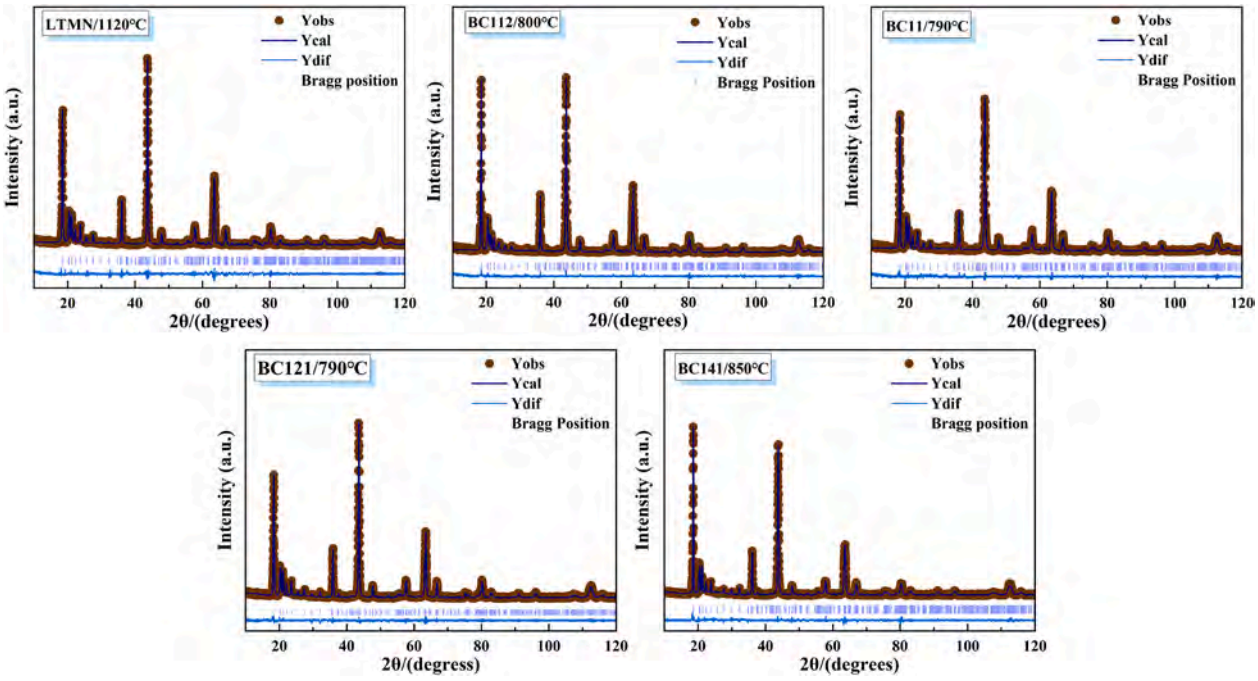

Fig. 2. Rietveld refinement patterns of five samples.

1.2:1.0) and BC141 (x:y = 1.4:1.0), orderly. Fourthly, the dried powders were mixed with 4 wt% paraffin, then the mixture was uniaxially pressed into cylinder (diameter ~ 10 mm, height ~ 4 mm). Finally, these samples were sintered at 750–870 °C in air for 4 h. To investigate the chemical compatibility between Ag and BC11 ceramic, the mixture of 25 wt% Ag powder and BC11 powders was sintered at 790 °C for 4 h.

The crystal phase of sintered specimens was investigated via X-ray diffraction with CuKα radiation (D/MAX-2500). The micro-surface morphology of sintered ceramics was observed using scanning electron microscopy (FE-SEM, S-4800). The Raman spectra of BC-doped LTMN specimens was recorded by a Raman spectrometer (Raman, DXR Microscope), which equipped with a 532 nm laser source. The lattice parameters of BC-doped LTMN ceramics were obtained by Rietveld refinement with GSAS software. The grain size was measured with Nano Measurer 1.2 software, and the bulk densities (ρ) of BC-doped LTMN specimens were measured via the Archimedes' method. The theoretical densities (ρ_{the}) and relative densities (ρ_{rel}) could be calculated according to following equations [31,32]:

$$\rho_{the} = \frac{AZ}{N_A V} \tag{3}$$

$$\rho_{rel} = \frac{\rho}{\rho_{the}} \times 100\% \tag{4}$$

where A represents atomic weight, and Z represents the number of molecules in a single unit cell. N_A and V are Avogadro constant and unit cell volume, respectively.

The relative dielectric constants (ε_r) of sintered samples were measured via Hakki-Coleman's method and characterized by network analyzer (Agilent 8720 ES). The transmission cavity method was used to test the quality factor (Q × f) with the network analyzer. The resonant frequencies of samples sintered at optimum temperature were measured in the temperature range of −40 °C–120 °C, and temperature coefficient (τ_f) of the resonant frequency was characterized with the following formula:

$$TCF(\tau_f) = \frac{(fT_2 - fT_1) \times 10^6}{fT_1(T_2 - T_1)} \tag{5}$$

where f_{T1} and f_{T2} are the resonance frequency of T_1 and T_2 temperature, respectively.

3. Results and discussion

The XRD patterns of BC-doped LTMN ceramics sintered at optimum temperature are shown in Fig. 1(a). All diffraction peaks could be indexed in terms of Li_2TiO_3 phase (JCPDS #33–0831). Although x:y changed from 1.0:1.2 to 1.4:1.0, extra peak was not detected in the curve of BC-doped LTMN, which indicated that the liquid phase of BC was not crystallized in LTMN ceramic and existed in the form of amorphous state after sintering process [1,33–35]. The second phase was also not detected in the XRD pattern of BC11 as the sintering temperature changed from 770 °C to 810 °C, as shown in Fig. 1(b). Moreover, the shift of (002) diffraction peak is displayed in Fig. 1(c). It could be observed that (002) diffraction peak gradually shifted to a low degree as the sintering temperature of the BC11 ceramic increased, which indicated an expansion in unit cell volume based on the Bragg's formula ($2d\sin\theta = n\lambda$) [36]. The lattice parameters and Rietveld refinement patterns of BC-doped LTMN ceramics are shown in Table 1 and Fig. 2, respectively. Notably, the Rietveld refinement further proved that the cell volume of BC11 expanded as the sintering temperature increased. This result may be attributed to the substitution of Li^+ and Ti^{4+} (the average ions radius of Li^+ and Ti^{4+}: R_{aver} = 0.708 Å) ions by Cu^{2+} ($R_{Cu^{2+}}$=0.73 Å) in BC11 ceramic.

Fig. 3 gives the Raman spectra of LTMN, BC112, BC11, BC121, and BC141 specimens sintered at the optimum temperatures, respectively. Based on the reported literatures [1,37–39], the distribution of Raman peak/band for Li_2TiO_3-based ceramics was summarized. The Raman peak at 212 cm^{-1} could be assigned to bending vibration of O–Ti–O, and 250-350 cm^{-1} could be attributed to the stretching vibration of Li–O and the bending vibration of O–Li–O. The Raman band at 550-700 cm^{-1}

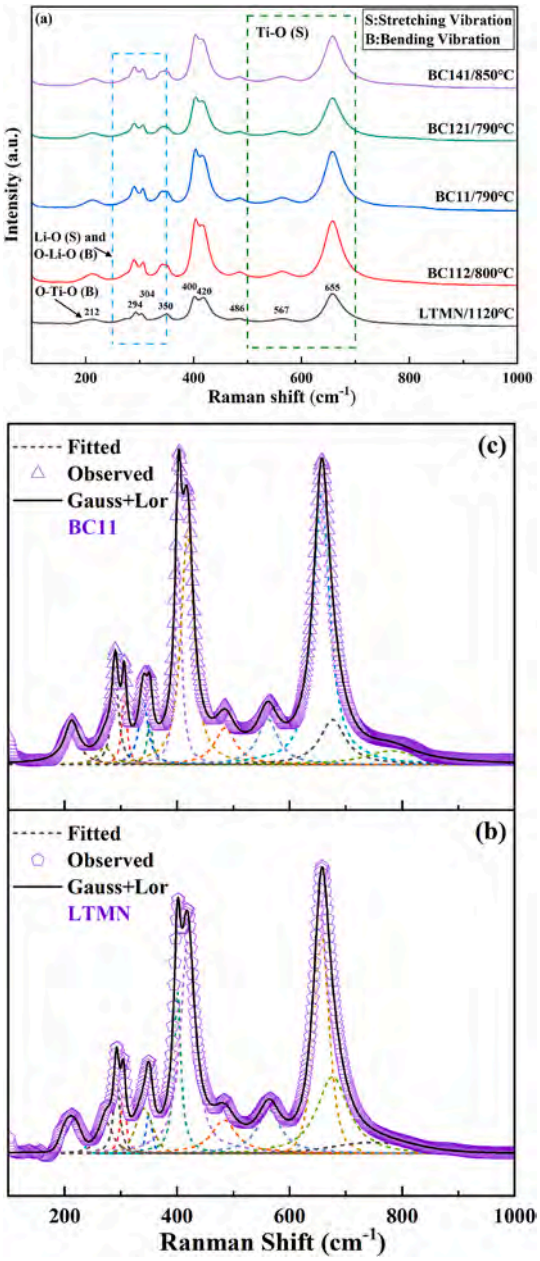

Fig. 3. (a) The Raman spectra of LTMN, BC112, BC11, BC121 and BC141 ceramics sintered at the optimum sintering temperature for 4 h, respectively. (b) and (c) The experimental (pentagon and triangle) and fitted (black solid line) Raman spectra of LTMN and BC11 ceramics sintered at optimal temperatures. (The short-dashed lines are the Gaussian-Lorentzian mode fitting).

Table 2
The full width at half maxima of five samples.

Samples	LTMN	BC112	BC11	BC121	BC141
$FWHM_{350cm^{-1}}$	13.169	13.198	13.525	13.749	15.391

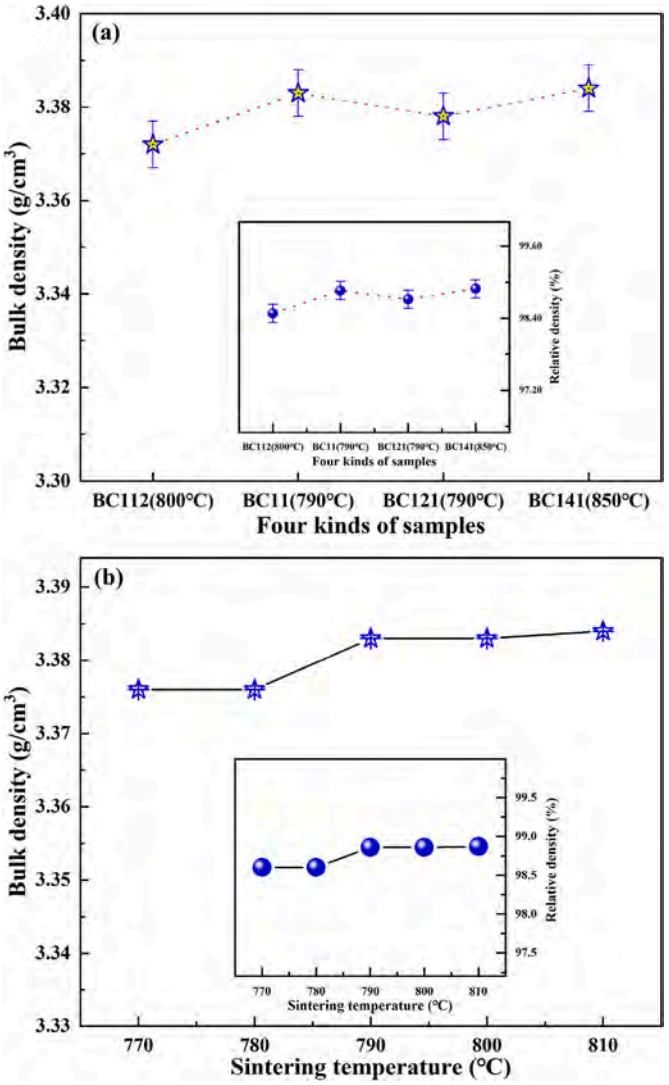

Fig. 4. (a) The bulk densities of BC112, BC11, BC121 and BC141 ceramics sintered at optimum temperature, respectively. (b) The bulk densities of BC11 ceramics as a function of sintering temperature. (The insets show the relative density of each BC-doped specimens).

could be regarded as the stretching vibration of Ti–O. As we all know, the Raman spectroscopy and Raman stretching modes are closely related to short-range order and neighboring disorder (such as electrical defects caused by substitutions or vacancies), respectively [22]. For example, the Raman peak of BC-modified LTMN ceramics slightly broadened at 350 cm^{-1} compared with pure LTMN, which might be related to a decrease in cation ordering [1]. The Raman fitting is shown in Fig. 3(b) and (c), and the fitted full width at half maxima (FWHM) information is listed in Table 2. As discussed above, the slight addition of BC could not affect the phase composition of LTMN ceramic, which was confirmed by Raman spectroscopy and X-ray diffraction, but it would have a slight impact on its microstructure.

Fig. 4(a) shows the bulk and relative densities of BC112, BC11, BC121, and BC11 ceramics sintered at optimum temperature, respectively. It could be observed that the bulk densities of four samples varied between 3.372 and 3.384 g/cm^3, and relative densities were located in 98.5%–98.8% (>95%), which indicated that BC-modified samples reached densification. Furthermore, the optimum sintering temperature was closely related to the composition of ceramic samples. It was observed that the optimum sintering temperature sharply increased from 790 °C to 850 °C as *x*:*y* changed from 1.0:1.2 to 1.4:1.0. Although the relative densities of BC141 and BC11 were very close, the sintering temperature of the former was nearly 60 °C higher than that of the latter. Therefore, BC11 was selected as a further research object, and the bulk and relative density of BC11 sintered at various temperatures were measured. Under the same mass ratio, the relative density of BC11

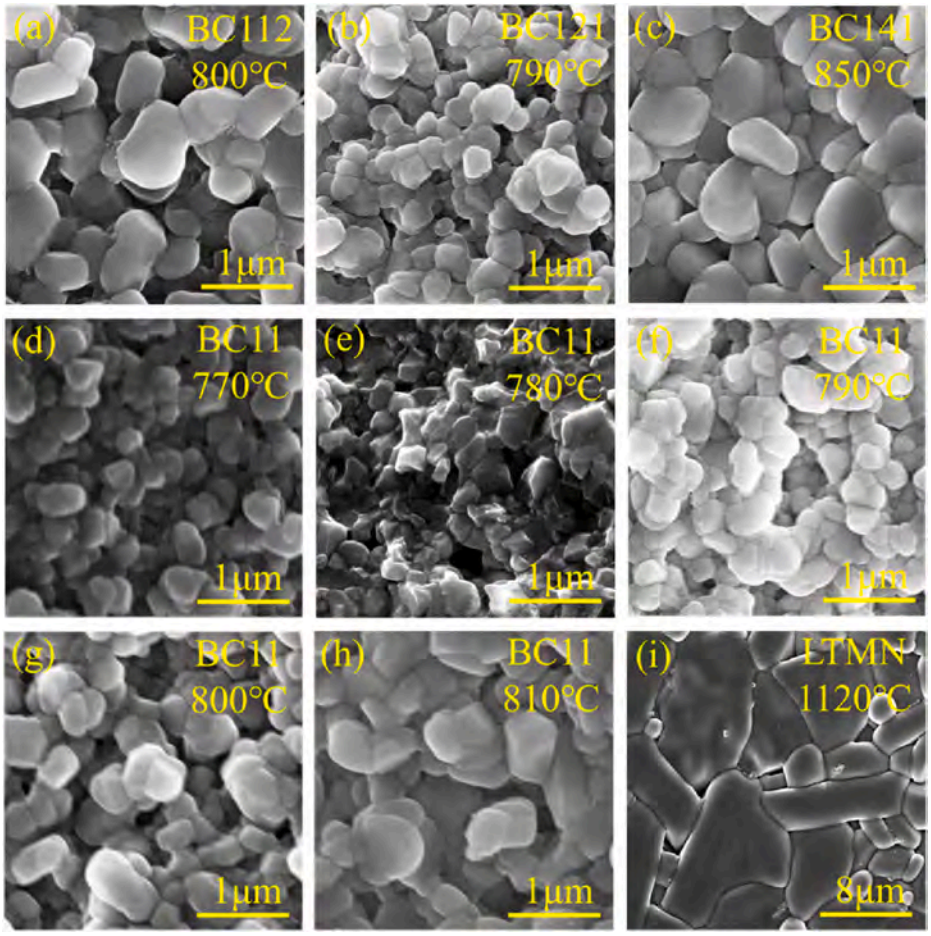

Fig. 5. (a)–(c) The SEM images of BC112, BC121, and BC141 ceramics sintered at optimum temperatures for 4 h, respectively. (d)–(h) Evolution of the microstructure with sintering temperature for the BC11 composition. (i) LTMN ceramics sintered at 1120 °C for 4 h.

ceramic changed slightly. When sintering temperature reached 780 °C, the relative density gradually increased, then a saturation value was obtained at 790 °C as shown in Fig. 4(b). This indicates that BC additive could effectively lower sintering temperature and promote the sinterability of LTMN specimen.

The SEM images of LTMN and BC-modified LTMN ceramics are shown in Fig. 5. Fig. 6(a)-(e) illustrate the grain-size distribution of BC-modified and LTMN ceramics. The grain size of BC-modified LTMN specimens was relatively smaller than LTMN due to the decrease in sintering temperature [40], but it was relatively uniform and well-arranged. Fig. 5(a)–(c) and (f) present the microtopography of the LTMN ceramic with the addition of different mass ratio of BC. When *x*:*y* was 1.0:1.2, the mean grain size of BC112 (0.66 μm) was relatively larger compared with BC11 (0.48 μm) and BC121 (0.41 μm), as shown in Fig. 5(a). When *x*:*y* increased to 1.0:1.0 and 1.2:1.0, the grains of BC11 and BC121 were arranged more uniformly, as shown in Fig. 5(f), (b). In Fig. 5(c), the microstructure became more compact and grains became more uniform when *x*:*y* is 1.4:1.0. This phenomenon indicated that the addition of BC was an effective method to accelerate the sintering process, help to achieve uniform grains, and lower the sintering temperature of LTMN specimen. Furthermore, the microstructural evolution of BC11 ceramic sintered at various temperatures is shown in Fig. 5(d)–(h). Some pores were left between the grains of BC11 ceramic sintered at 780 °C. As the sintering temperature rose to 790 °C, the pores in BC11 specimen gradually disappeared due to the growth of grains, and BC11 showed a tight and uniform arrangement of grains. A large amount of liquid phase was generated and some large pores appeared in BC11 specimen as the sintering temperature increased to 810 °C. This phenomenon may be caused by the evaporation of liquid phase during the sintering process [41]. In a word, a small amount of liquid phase was beneficial to the rearrangement and recrystallization of LTMN grains, while an excessive amount of liquid phase was harmful to sintering process.

Fig. 7 displays ε_r of BC-modified LTMN ceramics as functions of BC ratio and sintering temperature. The porosity-corrected dielectric constants (ε_{corr}) were also calculated to eliminate the effect of porosity [42]:

$$\varepsilon_r = \varepsilon_{corr}\left(1 - \frac{3p(\varepsilon_{corr} - 1)}{2\varepsilon_{corr} + 1}\right) \quad (6)$$

where ε_r and p are the measured dielectric constant and porosity, respectively. As *x*:*y* increased from 1.0:1.2 to 1.2:1.0, the ε_r fluctuated slightly between 23.5 and 24.44, and ε_{corr} changed between 24.36 and 24.75. With a fixed composition BC141, the ε_r of BC-modified samples increased with increasing sintering temperature, after that reached a saturate value ~24.5. The variation trend of ε_r in BC-modified specimens was similar to bulk density. A higher density for a ceramic body meant there were more dipoles in a unit volume and the ceramic was

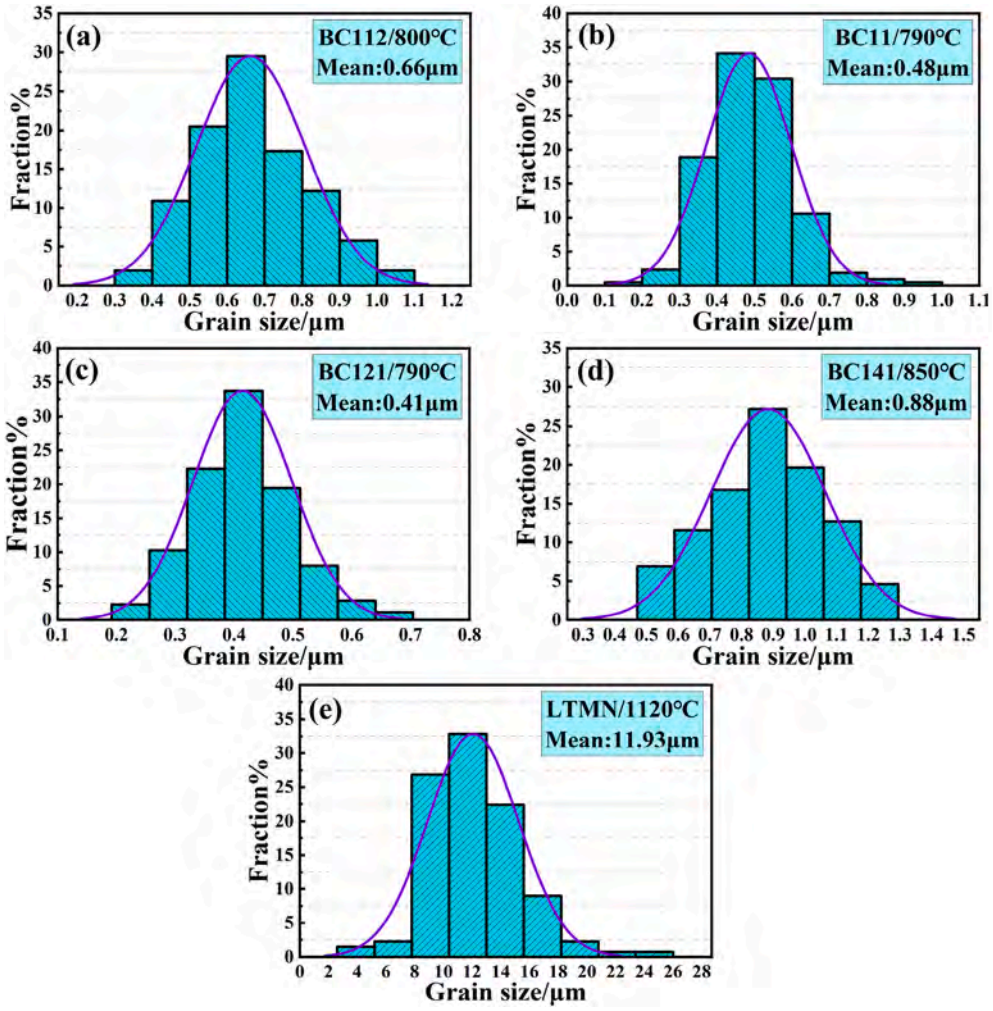

Fig. 6. Grain size distribution of BC-doped LTMN ceramics: (a) BC112, at 800 °C, (b) BC11, at 790 °C, (c) BC121, at 790 °C, (d) BC141, at 850 °C, (e) pure LTMN ceramic, at 1120 °C.

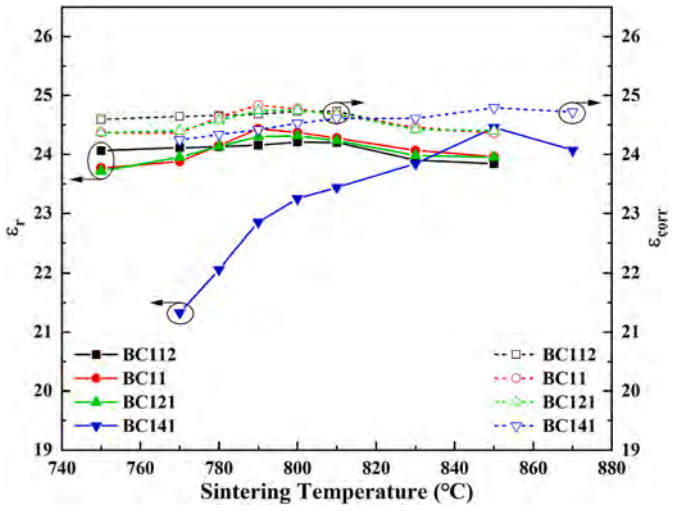

Fig. 7. Measured and porosity-corrected dielectric constants of LTMN ceramics with different BC additions as a function of sintering temperature.

easier to be polarized [43,44]. This result also indicated that the bulk density was the major factor to control ε_r in BC-doped LTMN ceramics. It was noteworthy that the ε_r displayed a slight decrease after reaching maximum value. This may be ascribed to two reasons. The first one was the density, which was shown in Fig. 4. The relative densities of BC-doped LTMN specimens reached about 98.5%, but some pores left in BC-doped specimens, which resulted in a decrease of ε_r. The second reason was the low ε_r of BC. The ε_r decreased due to the generation of excessive liquid phase with lower ε_r as exceeding the optimal sintering temperature.

The $Q \times f$ values of BC-doped LTMN ceramics followed a similar trend to the dielectric constants, as shown in Fig. 8. For BC11 ceramic, the optimized sintering temperature could be reduced to approximately 790 °C. Even sintered at 750 °C, BC11 ceramic still retained a higher $Q \times f$ value (51,636 GHz). The improvement of $Q \times f$ value may be closely

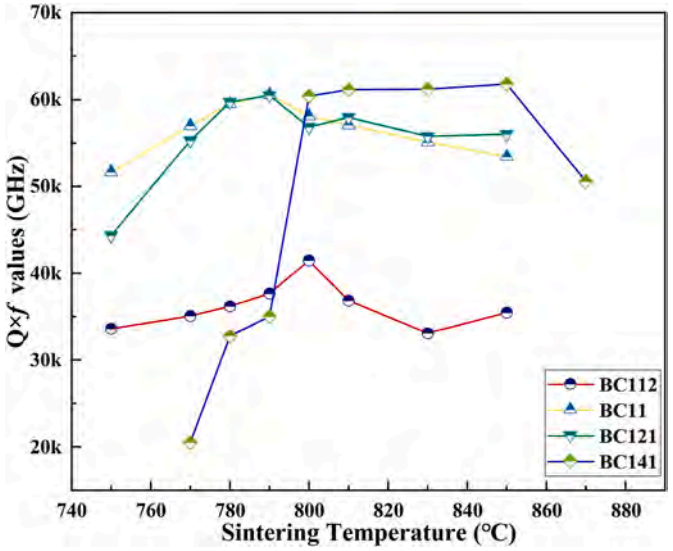

Fig. 8. The $Q \times f$ values of BC112, BC11, BC121, and BC141 ceramics as a function of sintering temperature, respectively.

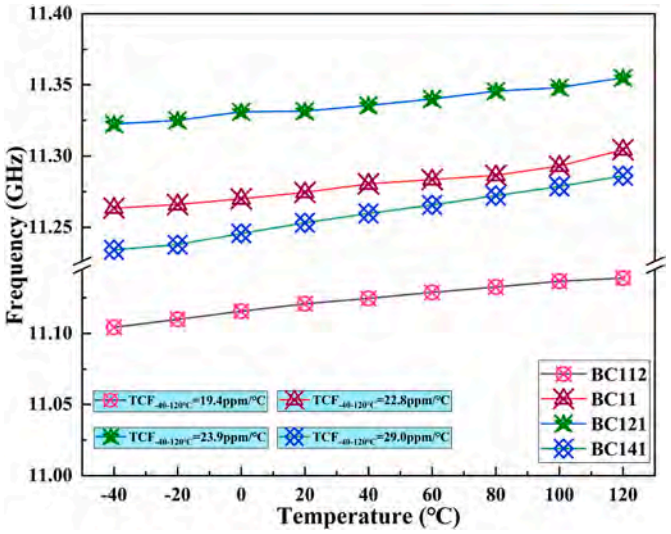

Fig. 9. The resonant frequencies of BC112(800 °C), BC11(790 °C), BC121 (790 °C), and BC141(850 °C) specimens sintered at optimum temperature as a function of measured temperature.

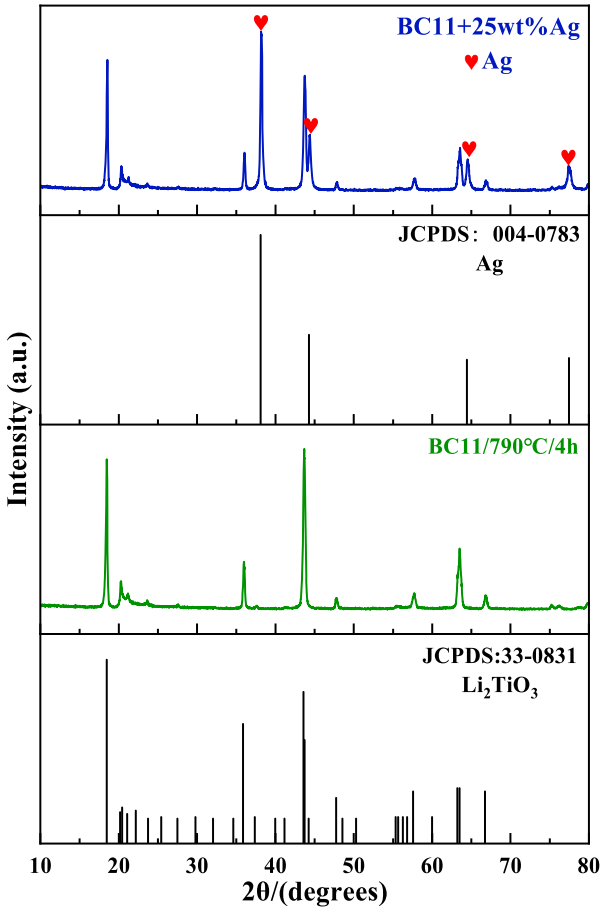

Fig. 10. The XRD patterns of BC11 ceramic doped with 25 wt% Ag powder sintered at 790 °C for 4 h.

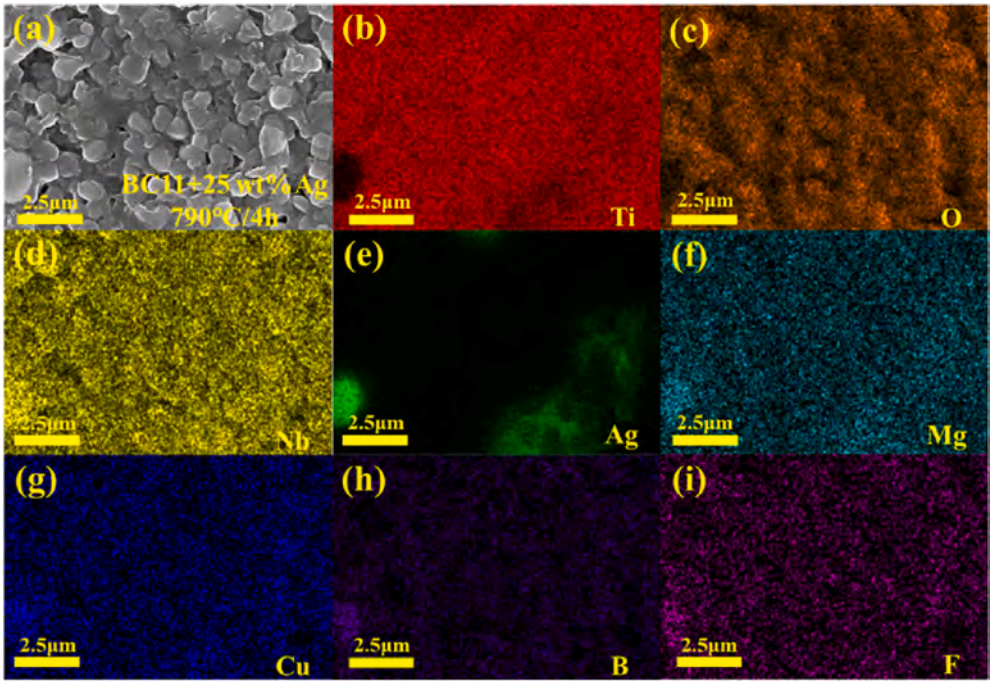

Fig. 11. The SEM images of (a) BC11 ceramic with 25 wt% Ag powder and corresponding EDS analysis surface scanning of (b) Ti element (c) O element (d) Nb element (e) Ag element (f) Mg element (g) Cu element (h) B element (i) F element.

related to the growth of grains, since larger grain-size specimens had fewer boundaries that were harmful to dielectric performances. As shown in Fig. 8, the $Q \times f$ value of BC141 increased with increasing sintering temperature and reached the maximum of 61,801 GHz at 850 °C. The dielectric loss at microwave frequency can be attributed to intrinsic and extrinsic losses; The intrinsic losses were mainly controlled by lattice vibration modes, and the external loses were influenced by many factors, such as second phases, oxygen vacancies, grain sizes and densification [45]. As shown in Figs. 5(c) and Fig. 6(d), the most compact and uniform arrangement of grains were obtained in BC141 ceramic, which explained that the optimum $Q \times f$ value was achieved in BC141.

Fig. 9 displays the τ_f values of BC-modified LTMN ceramics sintered at optimum temperatures. As the temperature increased, a slight change in resonant frequency and an insignificant change in τ_f were observed. When *x*:*y* changed from 1.0:1.2 to 1.0:1.0, the τ_f value of BC-doped LTMN ceramic increased from 19.4 to 22.8 ppm/°C. When *x*:*y* were 1.2:1.0 and 1.4:1.0, the τ_f values for BC121 and BC141 ceramics were 23.9 and 29.0 ppm/°C, respectively.

The sintering temperature (maximum 850 °C) of BC-doped LTMN is obviously lower than the melting point of silver (961 °C). The sintering temperature met the requirement of LTCC technology, but the chemical compatibility between ceramics and Ag electrodes was more important in the manufacture of LTCC devices [46]. Therefore, 25 wt% Ag powder and BC11 were uniformly mixed and co-fired at 790 °C in air ambient atmosphere for 4 h to verify the chemical compatibility between them. The XRD pattern of BC11 composition with Ag is illustrated in Fig. 10. It could be observed that no impurity phase appeared except for BC11 and Ag (JCPDS: 004–0783) diffraction phases. This result indicated that no additional phases were formed during the sintering process, and no chemical reaction occurred between BC11 and Ag, which was also confirmed by EDS elemental mapping analysis in Fig. 11(a)-(i). Among them, the bright color represented the Ag phase in Fig. 11(e).

A summarization of the $Q \times f$ versus sintering temperature (ST) is illustrated for Li_2TiO_3-based [1,33,46,52,53,55–61,63] and some other low ST MWDCs [29,41,47–51,54,62], as shown in Fig. 12(a). Compared with the microwave dielectric properties of Li_2TiO_3-based ceramics reported in other literatures, it is easy to find that the ST of BC11 ceramic (with a higher $Q \times f$ value) is the lowest. Fig. 12(b) summarizes the dielectric performance (ε_r and ST) for these materials [1,33,41,46,48–67]. The dielectric constant of BC11 ceramic is located in the central position of Fig. 12(b). It can be seen that BC11 has suitable dielectric constant, which is conducive to achieve the miniaturization of communication devices and lower the time-delay of signals transmission. Besides, the extremely low ST can not only meet the needs of co-firing with the Ag electrode but also cater to the concept of energy-saving. In short, BC11 ceramic stand out among the reported LTCC materials due to its comprehensively superior performances.

4. Conclusion

In this paper, microstructure evolution, phase composition, and microwave dielectric performance of BC-doped LTMN specimens were studied systematically. It can be seen that the addition of BC could lower the sintering temperature of LTMN specimen to 790 °C without an evident decrease in microwave dielectric performance. For example, BC11 ceramic sintered at 790 °C exhibited superior microwave dielectric properties of ε_r ~24.44, $Q \times f$ ~60,574 GHz and τ_f ~22.8 ppm/°C. Furthermore, excellent microwave properties of ε_r ~23.77 and $Q \times f$ ~51,636 GHz were achieved in BC11 ceramic sintered at 750 °C, which was 370 °C lower than pure LTMN ceramic. Moreover, the great chemical compatibility between BC-doped LTMN ceramics and Ag was proved by XRD and EDS energy spectrum. This result reveals that BC-doped LTMN ceramics are a promising candidate for 5G LTCC materials.

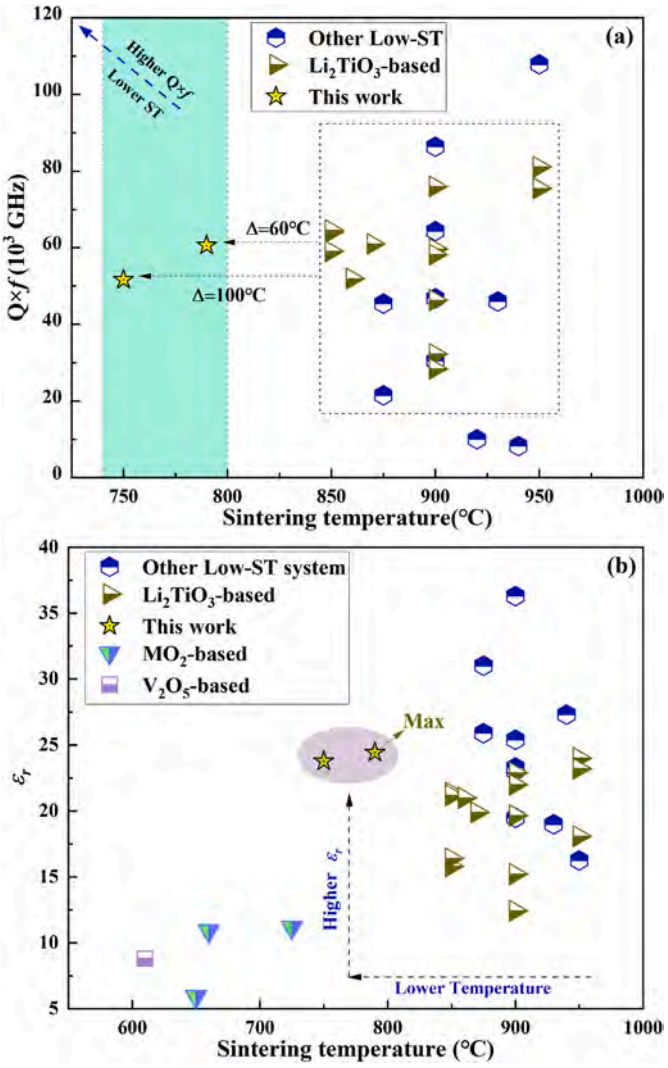

Fig. 12. Summary of Q × *f* and ε_r values versus sintering temperature plot for low sintering temperature system.

Declaration of competing interest

The authors declare that they have no known competing financial interests or personal relationships that could have appeared to influence the work reported in this paper.

Acknowledgements

This work was supported by the National Key R&D Program of China (Grant no. 2017YFB0406300). The authors thank Mr Jianli Qiao for his help in using Raman spectrometer (Raman, DXR Microscope, Thermo Fisher, USA).

References

[1] H.H. Guo, D. Zhou, C. Du, et al., Temperature stable $Li_2Ti_{0.75}(Mg_{1/3}Nb_{2/3})_{0.25}O_3$-based microwave dielectric ceramics with low sintering temperature and ultra-low dielectric loss for dielectric resonator antenna applications, J. Mater. Chem. C. 8 (2018) 4690–4700.

[2] X.Q. Song, W. Lei, Y.Y. Zhou, et al., Ultra-low fired fluoride composite microwave dielectric ceramics and their application for $BaCuSi_2O_6$-based LTCC, J. Am. Ceram. Soc. 103 (2020) 1140–1148.

[3] H.S. Ren, S.H. Jiang, M.Z. Dang, et al., Investigating on sintering mechanism and adjustable dielectric properties of BLMT glass/$Li_2Zn_3Ti_4O_{12}$ composites for LTCC applications, J. Alloys Compd. 740 (2018) 1188–1196.

[4] Y.W. Chen, E.Z. Li, S.X. Duan, et al., Low temperature sintering kinetics and microwave dielectric properties of $BaTi_5O_{11}$ ceramic, ACS Sustain. Chem. Eng. 5 (2017) 10606–10613.

[5] X.K. Lan, Z.Y. Zou, W.Z. Lu, et al., Phase transition and low-temperature sintering of $Zn(Mn_{1-x}Al_x)_2O_4$ ceramics for LTCC applications, Ceram. Int. 42 (2016) 17731–17735.

[6] D.W. Wang, S.Y. Zhang, G. Wang, et al., Cold sintered $CaTiO_3$-K_2MoO_4 microwave dielectric ceramics for integrated microstrip patch antennas, Appl. Mater. Today. 18 (2020) 100519.

[7] J. Zhang, Z.X. Yue, Y. Luo, et al., Novel low-firing forsterite-based microwave dielectric for LTCC applications, J. Am. Ceram. Soc. 99 (2016) 1122–1124.

[8] D. Zhou, L.X. Pang, D.W. Wang, et al., High permittivity and low loss microwave dielectrics suitable for 5G resonators and low temperature co-fired ceramic architecture, J. Mater. Chem. C. 5 (2017) 10094–10098.

[9] T. Sun, B. Xiao, F. Jin, et al., Ultralow-loss (1-x)$CaWO_4$-xNa_2WO_4 (x= 0.1, 0.2) microwave dielectric ceramic for LTCC applications, J. Materiomics (2021), https://doi.org/10.1016/j.jmat.2021.02.006.

[10] C.F. Tseng, P.H. Chen, P.A. Lin, Low temperature sintering and microwave dielectric properties of $Zn_{0.5}Ti_{0.5}NbO_4$ ceramics with ZnO additive for LTCC applications, J. Alloys Compd. 632 (2015) 810–815.

[11] X.K. Lan, J. Li, F. Wang, et al., A novel low-permittivity $LiAl_{0.98}(Zn_{0.5}Si_{0.5})_{0.02}O_2$-based microwave dielectric ceramics for LTCC application, Int. J. Appl. Ceram. Technol. 17 (2020) 745–750.

[12] J.I. Steinberg, S.J. Horowitz, R.J. Bacher, Low-temperature cofired tape dielectric material systems for multilayer interconnections, Microelectron. Int. 3 (1986) 36–39.

[13] K. Ju, H.T. Yu, L. Ye, et al., Ultra-low temperature sintering and dielectric properties of SiO_2-filled glass composites, J. Am. Ceram. Soc. 96 (2013) 3563–3568.

[14] C.L. Chen, W.C.J. Wei, A. Roosen, Wetting, densification and phase transformation of $La_2O_3/A_2O_3/B_2O_3$-based glass–ceramics, J. Eur. Ceram. Soc. 26 (2006) 59–65.

[15] S. Arcaro, F.R. Cesconeto, F. Raupp-Pereira, et al., Synthesis and characterization of LZS/α-Al_2O_3 glass-ceramic composites for applications in the LTCC technology, Ceram. Int. 40 (2014) 5269–5274.

[16] G.B. Xia, L. He, D.A. Yang, Preparation and characterization of CaO–Al_2O_3–SiO_2 glass/fused silica composites for LTCC application, J. alloy. Comp. 531 (2012) 70–76.

[17] D. Thomas, P. Abhilash, M.T. Sebastian, Casting and characterization of $LiMgPO_4$ glass free LTCC tape for microwave applications, J. Eur. Ceram. Soc. 33 (2013) 87–93.

[18] P. Abhilash, D. Thomas, K.P. Surendran, et al., Facile synthesis of "Quench-Free Glass" and ceramic-glass composite for LTCC applications, J. Am. Ceram. Soc. 96 (2013) 1533–1537.

[19] P. Abhilash, M.T. Sebastian, K.P. Surendran, Glass free, non-aqueous LTCC tapes of $Bi_4(SiO_4)_3$ with high solid loading, J. Eur. Ceram. Soc. 35 (2015) 2313–2320.

[20] Y. Yang, M.S. Ma, F.Q. Zhang, et al., Low-temperature sintering of Al_2O_3 ceramics doped with 4CuO-TiO_2-2Nb_2O_5 composite oxide sintering aid, J. Eur. Ceram. Soc. 40 (2020) 5504–5510.

[21] D. Zhou, H. Wang, L.X. Pang, et al., Bi_2O_3–MoO_3 binary system: an alternative ultralow sintering temperature microwave dielectric, J. Am. Ceram. Soc. 92 (2009) 2242–2246.

[22] J.J. Bian, D.W. Kim, K.S. Hong, Glass-free LTCC microwave dielectric ceramics, Mater. Res. Bull. 40 (2005) 2120–2129.

[23] G.G. Yao, P. Liu, H.W. Zhang, Novel series of low-firing microwave dielectric ceramics: $Ca_5A_4(VO_4)_6$(A^{2+}= Mg, Zn), J. Am. Ceram. Soc. 96 (2013) 1691–1693.

[24] J. Zhang, R.Z. Zuo, Effect of ordering on the microwave dielectric properties of spinel-structured $(Zn_{1-x}(Li_{2/3}Ti_{1/3})_x)_2TiO_4$ ceramics, J. Am. Ceram. Soc. 99 (2016) 3343–3349.

[25] W. Wang, L.Y. Li, S.M. Xiu, et al., Microwave dielectric properties of $(Mg_{0.4}Zn_{0.6})_2SiO_4$–$CaTiO_3$ ceramics sintered with Li_2CO_3–H_3BO_3 for LTCC technology, J. Alloys Compd. 639 (2015) 359–364.

[26] A. Surjith, R. Ratheesh, High Q ceramics in the $ACe_2(MoO_4)_4$ (A= Ba, Sr and Ca) system for LTCC applications, J. alloy. Comp. 550 (2013) 169–172.

[27] S. Chen, W. Li, D.G. Zhu, Sintering behaviors, phases, and dielectric properties of MO-TeO_2-V_2O_5 (M= Ca, Sr, Ba) ultralow temperature ceramics, Mater. Res. Bull. 101 (2018) 29–38.

[28] X.Y. Ding, H. Wang, H.F. Zhou, et al., Microwaves dielectric properties of 3Li_2O-Nb_2O_5-6TiO_2 ceramics with B_2O_3 addition, Ferroelectrics 407 (2010) 93–100.

[29] Y. Zhang, Y.C. Zhang, M.Q. Xiang, et al., Low temperature sintering and microwave dielectric properties of $CoTiNb_2O_8$ ceramics with CuO addition, Ceram. Int. 42 (2016) 3542–3547.

[30] P. Zhang, J.W. Liao, Y.G. Zhao, et al., Effects of B_2O_3 addition on the sintering behavior and microwave dielectric properties of $Li_3Mg_2NbO_6$ ceramics, J. Mater. Sci. Mater. Electron. 28 (2017) 686–690.

[31] X. Zhang, Z. Fang, H. Yang, et al., Lattice evolution, ordering transformation and microwave dielectric properties of rock-salt $Li_{3+x}Mg_{2-2x}Nb_{1-x}Ti_{2x}O_6$ solid-solution system: a newly developed pseudo ternary phase diagram, Acta Mater. 206 (2021) 116636.

[32] Y. Zhan, L.X. Li, Low-permittivity and high-Q value $Li_2Mg_3Ti_{1-x}(Zn_{1/3}Nb_{2/3})_xO_6$ microwave dielectric ceramics for microstrip antenna applications in 5G millimeter wave, J. Alloys Compd. 857 (2021) 157608.

[33] J. Liang, W.Z. Lu, Microwave dielectric properties of Li_2TiO_3 ceramics doped with ZnO–B_2O_3 frit, J. Am. Ceram. Soc. 92 (2009) 952–954.

[34] L.X. Pang, H. Liu, D. Zhou, et al., Low-temperature sintering and microwave dielectric properties of Li_3MO_4 (M= Ta, Sb) ceramics, J. Alloys Compd. 525 (2012) 22–24.

[35] Y. Wu, R.Z. Zuo, J.J. Zhang, et al., Influence of CuO and B_2O_3 on sintering and dielectric properties of tungsten bronze type microwave ceramics: a case study in $Ba_4Nd_{9.3}Ti_{18}O_{54}$, J. Mater. Sci. Mater. Electron. 22 (2011) 106–110.
[36] M.K. Du, L.X. Li, S.H. Yu, et al., High-Q microwave ceramics of Li_2TiO_3 co-doped with magnesium and niobium, J. Am. Ceram. Soc. 101 (2018) 4066–4075.
[37] L.H. Robins, D.L. Kaiser, L.D. Rotter, et al., Investigation of the structure of barium titanate thin films by Raman spectroscopy, J. Appl. Phys. 76 (1994) 7487–7498.
[38] A. Li, C.Z. Ge, P. Lü, D. Wu, et al., Fabrication and electrical properties of sol-gel derived $BaTiO_3$ films with metallic $LaNiO_3$ electrode, Appl. Phys. Lett. 70 (1997) 1616–1618.
[39] T. Nakazawa, A. Naito, T. Aruga, et al., High energy heavy ion induced structural disorder in Li_2TiO_3, J. Nucl. Mater. 367 (2007) 1398–1403.
[40] D.L. Corker, R.W. Whatmore, E. Ringgaard, et al., Liquid-phase sintering of PZT ceramics, J. Eur. Ceram. Soc. 20 (2000) 2039–2045.
[41] J.B. Lim, D.H. Kim, S. Nahm, et al., Effect of B_2O_3 and CuO additives on the sintering temperature and microwave dielectric properties of $Ba(Mg_{1/3}Nb_{2/3})O_3$ ceramics, Mater. Res. Bull. 41 (2006) 1199–1205.
[42] G. Wang, D.N. Zhang, J. Li, et al., Crystal structure, bond energy, Raman spectra, and microwave dielectric properties of Ti-doped $Li_3Mg_2NbO_6$ ceramics, J. Am. Ceram. Soc. 103 (2020) 4321–4332.
[43] H.K. Li, W.Z. Lu, W. Lei, Microwave dielectric properties of $Li_2ZnTi_3O_8$ ceramics doped with ZnO–B_2O_3 frit, Mater. Lett. 71 (2012) 148–150.
[44] J. Zhang, R.Z. Zuo, A novel self-composite property-tunable $LaTiNbO_6$ microwave dielectric ceramic, Mater. Res. Bull. 83 (2016) 568–572.
[45] M.J. Wu, J.D. Chen, Y.C. Zhang, Effect of B_2O_3 addition on the microwave dielectric properties of $NiTiNb_2O_8$ ceramics, J. Mater. Sci. Mater. Electron. 29 (2018) 13132–13137.
[46] L.X. Pang, D. Zhou, Microwave dielectric properties of low-firing Li_2MO_3 (M= Ti, Zr, Sn) ceramics with B_2O_3–CuO addition, J. Am. Ceram. Soc. 93 (2010) 3614–3617.
[47] C.M. Cheng, S.H. Lo, C.F. Yang, The effect of CuO on the sintering and properties of BiNbO4 microwave ceramics, Ceram. Int. 26 (2000) 113–117.
[48] Y. Bao, G.H. Chen, M.Z. Hou, et al., Microwave dielectric properties and compatibility with silver of low-fired $Li_2MgTi_3O_8$ ceramics with Li_2O-MgO-B_2O_3 frit, T. Nonferr. Metal. Soc. 23 (2013) 3318–3323.
[49] Y.C. Lee, W.H. Leeb, F.S. Shieuc, Microwave dielectric properties and microstructures of Ba2Ti9O20-based ceramics with 3ZnO–B_2O_3 addition, J. Eur. Ceram. Soc. 25 (2005) 3459–3468.
[50] J.B. Lim, S. Nahm, H.T. Kim, et al., Effect of B_2O_3 and CuO on the sintering temperature and microwave dielectric properties of the $BaTi_4O_9$ ceramics, J. Electroceram. 17 (2006) 393–397.
[51] D. Zhou, H. Wang, L.X. Pang, et al., Low temperature firing of $BiSbO_4$ microwave dielectric ceramic with B_2O_3–CuO addition, J. Eur. Ceram. Soc. 29 (2009) 1543–1546.
[52] G.H. Chen, M.Z. Hou, Y. Yang, Microwave dielectric properties of low-fired Li_2TiO_3 ceramics doped with Li_2O–MgO–B_2O_3 frit, Mater. Lett. 89 (2012) 16–18.
[53] Y.Z. Hao, H. Yang, G.H. Chen, et al., Microwave dielectric properties of Li_2TiO_3 ceramics doped with LiF for LTCC applications, J. Alloys Compd. 552 (2013) 173–179.
[54] X.P. Lu, Y. Zheng, Z.W. Dong, et al., Low temperature sintering and microwave dielectric properties of $0.6Li_2ZnTi_3O_8$–$0.4Li_2TiO_3$ ceramics doped with ZnO–B_2O_3–SiO_2 glass, Mater. Lett. 131 (2014) 1–4.
[55] J.L. Ma, Z.F. Fu, P. Liu, et al., Microwave dielectric properties of low-fired Li_2TiO_3–MgO ceramics for LTCC applications, Mater. Sci. Eng. B-Adv. 204 (2016) 15–19.
[56] S.A. Sayyadi, T.E. Nassaj, S.A.H. Tabrizi, et al., Microwave dielectric properties and chemical compatibility with silver electrode of Li_2TiO_3 ceramic with Li_2O–ZnO–B_2O_3 glass additive, Physica B 457 (2015) 57–61.
[57] S. Zhang, H. Su, H. Zhang, et al., Microwave dielectric properties of $CaWO_4$–Li_2TiO_3 ceramics added with LBSCA glass for LTCC applications, Ceram. Int. 42 (2016) 15242–15246.
[58] W. Zhen, S. Li, J.J. Bian, Low temperature sintering and microwave dielectric properties of Li_2TiO_3–Li_2WO_4 composite ceramics, Ceram. Int. 39 (2013) 9767–9772.
[59] W.Q. Liu, R.Z. Zuo, A novel Li_2TiO_3–Li_2CeO_3 ceramic composite with excellent microwave dielectric properties for low-temperature cofired ceramic applications, J. Eur. Ceram. Soc. 38 (2018) 119–123.
[60] H.Z. Zuo, X.L. Tang, H. Guo, et al., Effects of $BaCu(B_2O_5)$ addition on microwave dielectric properties of Li_2TiO_3 ceramics for LTCC applications, Ceram. Int. 43 (2017) 13913–13917.
[61] H.H. Guo, M.S. Fu, D. Zhou, et al., Design of a high-efficiency and-gain antenna using novel low-loss, temperature-stable $Li_2Ti_{1-x}(Cu_{1/3}Nb_{2/3})_xO_3$ microwave dielectric ceramics, ACS Appl. Mater. Interfaces 13 (2021) 912–923.
[62] B.J. Tao, W.F. Wang, H.Y. Liu, et al., Low-temperature sintering LiF-doped $Li_4Mg_3[Ti_{0.6}(Mg_{1/3}Nb_{2/3})_{0.4}]_2O_9$ microwave dielectric ceramics for LTCC applications, Ceram. Int. 47 (2021) 2584–2590.
[63] A.S. Shahraki, E.T. Nassaj, S.A. Tabrizi, et al., A new temperature stable microwave dielectric ceramic with low-sintering temperature in Li_2TiO_3–$Li_2Zn_3Ti_4O_{12}$ system, J. alloy. Comp. 597 (2014) 161–166.
[64] C.L. Huang, J.N. Liou, M.H. Tsai, et al., Microwave dielectric properties of $Li_2M_2(MoO_4)_3$ (M= Co, Ni) for LTCC applications, J. Am. Ceram. Soc. 2 (2020) 130–139.
[65] J.Q. Ren, K. Bi, X.L. Fu, et al., Novel Bi_2O_3-added $Al_2Mo_3O_{12}$ composite microwave dielectric ceramics for ULTCC applications, J. Alloys Compd. 823 (2020) 153867.
[66] H.C. Yang, S.R. Zhang, H.Y. Yang, et al., $Gd_2Zr_3(MoO_4)_9$ microwave dielectric ceramics with trigonal structure for LTCC application, J. Am. Ceram. Soc. 103 (2020) 1131–1139.
[67] C.L. Huang, J.L. Huang, M.H. Tsai, Ultra-low temperature sintering and temperature stable microwave dielectrics of $(Mg_{1-x}Zn_x)V_2O_6$(x=0-0.09) ceramics, J. Asian. Ceram. Soc. 9 (2020) 1–7.